C-RED 2 ER: high speed extended range InGaAs cameras

Isaure de Kernier* [a], Yann Wanwanscappel [a], David Boutolleau [a], Thomas Carmignani [a], Fabien Clop[a], Philippe Feautrier [a], J.L. Gach [a], Stephane Lemarchand [a], Eric Stadler [a]

[a] First Light Imaging S.A.S., Europarc Ste Victoire, Route de Valbrillant, 13590 Meyreuil, France;

* isaure.dekernier@first-light.fr; phone +33 442612920; www.first-light-imaging.fr

ABSTRACT

MCT-based cameras are very competitive when it comes to ultra-low light imaging, however it is crucial for less demanding applications to have a non-cryogenic and cost-effective solution. Progress in band-gap engineering has enabled to shift the detection cut-off wavelength of InGaAs by tuning the indium composition of the $In_xGa_{1-x}As$ compound. Operating with a double TEC coupled to air and water cooling, the C-RED 2 Extended Range cameras are an alternative to MCT for specific applications in astronomy and free space optics. We will present the performances of these new VGA extended range InGaAs cameras with sensitivity from 1.1 µm to 1.9 µm and from 1.2 µm to 2.2 µm.

Keywords: fast infrared cameras, extended range, InGaAs, imaging, sensing

1. INTRODUCTION

When it comes to detecting wavelength in the SWIR region, but beyond the 1.7 µm cutoff wavelength of InGaAs, HgCdTe (MCT) is often considered. Cameras based on MCT sensors offer a sensitivity range spanning from 0.8 to 2.5 µm. However, their mass production is complex: poor material uniformity low yield, high cost, *etc.* Additionally, because of their large dark current, MCT detectors need to be cooled down, often to temperatures requiring the use of cryogenics solutions. This is a major constraint on the set-up complexity and limits the relevance of this solution for applications that do not require ultra-high performance, typically for laboratory benchtop experiments.

As potential alternatives to MCT, other sensor technologies are available and significant progress has been made in new detector architecture [1]. For example, quantum dots sensors. These are engineered from a solution suspension of semiconductor quantum materials [4]. The spectral bandgap is tunable, and commercially available camera were reported with a wide bandwidth of 400 to 2000 µm. Low quantum efficiency is the main drawback of this technology.

Type II super lattice (T2SL) detector technology, first introduced in the 1980's, is based on stacking nanometric layers of semiconductor materials [2], [3]. It is a versatile solution as it enables to finely tune the cutoff wavelength from SWIR to LWIR by engineering the thickness and composition of individual layers. Although the technology is theoretically promising, available cameras still report high dark current. Hence, T2SL-based cameras require deep cooling, typically below 200K.

InGaAs sensors are fabricated by growing a crystalline layer of InGaAs on an indium phosphate (InP) substrate. In the case when the substrate has the same lattice constant as the alloy, resulting in lattice-matching, the detector absorbs light in the short-wave infrared region with a long cutoff wavelength at 1700 nm. This was first reported by Pearsall and colleagues in 1977 [5]. Introducing a higher fraction of indium in the ternary compound decreases the bandgap of the material and hence enables to shift the sensitivity curve to longer wavelengths. $In_xGa_{x-1}As$ with a longer cutoff wavelength is referred to as "extended range InGaAs". In this paper we are interested in extended range InGaAs obtained from In-rich InGaAs grown on InP substrate. This technology benefits from the maturity of standard InGaAs based detectors. The easy integration and no need for deep cooling makes it particularly attractive for benchtop applications.

We report in this paper the integration of such extended range detectors in a readily available camera.

2. THE C-RED 2 ER CAMERAS

2.1 Camera overview

C-RED 2 ER is designed for high performance imaging at wavelengths beyond the standard cutoff wavelength of InGaAs. The camera is based on the technological bricks developed at First Light Imaging for the C-RED 2 camera [6, p. 2], [7, p. 2].

C-RED 2 integrates a SNAKE detector from Lynred [8] and offers high-end performances particularly in terms of speed for applications such as Natural Guide Star (NGS) infrared wavefront sensing. The mechanical design of the camera is well suited for benchtop application. The C-RED 2 ER has the same form factor as C-RED 2, dimensions are H55 x W75 x L140 mm for 0.9 kg. The optical interface of both cameras is a standard C-mount.

Two detectors, commercially available from Andanta GmbH, are selected for the extended range camera: the BADGER-1.9-T2 and the BADGER-2.2-T2.

Figure 1. The C-RED 2 ER camera commercialized by First Light Imaging.

The figures of merit of the C-RED 2 ER cameras are referenced in the table below.

Table 1 – Main features of the C-RED 2 ER cameras

	C-RED 2 ER 1.9µm	**C-RED 2 ER 2.2µm**
Detector reference	BADGER-1.9-T2	BADGER-2.2-T2
Sensor size	640 x 512	
Pixel pitch	15 µm	
Sensitivity range	1.1 µm to 1.9 µm	1.2 µm to 2.2 µm
Maximum speed (full frame)	602 fps	
Maximum speed (24 x 4 window)	32 066 fps	
Quantization	14 bits	
Peak quantum efficiency	82%	83%
Detector operating temperature	-40 °C	-55°C

The sensor temperature is monitored and can reach high stabilization over time. The camera uses double stage thermoelectric cooling (TEC-2) system and additional air cooling to dissipate the heat away from the TEC hot side. The fan can be turned off for applications sensitive to vibrations. The camera integrates a water circuit inside the camera body. In a standard environment, this enables to bring the sensor temperature down to -55°C, with 20°C water.

2.2 C-RED 2 ER framerate

The C-RED 2 ER cameras allow for real-time applications, with two possible data interfaces: Camera Link® full and superspeed USB 3.

The camera is capable of windowing, allowing for increased image rate while maintaining a very low noise. Due to the USB 3 constraints, framerates above 9999 fps in windowing mode can only be achieved using the Camera Link® interface. Table 2 shows the C-RED 2 ER maximum framerates in windowing mode. In full frame (640 x 512 pixels), 600 frames per second can be reached. Ultra-fast framerates up to 32066 Hz can be reached for a 4 x 32 pixels window.

Table 2: Maximum framerates, in Hz, in windowing mode CDS readout (with Camera Link®)

		Columns					
		32	**64**	**128**	**256**	**512**	**640**
Lines	**4**	32066	31512	30458	28548	25367	24029
	8	28108	27348	25945	23532	19840	18397
	16	22542	21631	20015	17413	13819	12526
	32	16147	15254	13736	11455	8599	7646
	64	10302	9596	8440	6801	4898	4297
	128	5975	5509	4765	3752	2632	2291
	256	3247	2975	2547	1978	1367	1184
	512	1697	1549	1319	1016	397	602

3. QUANTUM EFFICIENCY

For a camera, quantum efficiency is the ratio of incident photons to photo-induced electrons. The photoelectric effect in semiconductor materials will convert a photon to an electron only if it has sufficient energy. The bandgap energy is an intrinsic feature of the material. The fact that the bandgap of HgCdTe is a function of cadmium composition is already widely used to engineer the sensitivity of MCT detectors. Similarly, the tuning the fraction of indium enables bandgap engineering on InGaAs detectors. For these extended range cameras, the quantum efficiency on the edges of the sensitivity range is of particular interest.

2.1 Quantum efficiency at room temperature

The quantum efficiency of the detectors at 20°C is shown in Figure 2, below. Both detectors have a peak quantum efficiency that exceeds 80% and a large plateau exceeding 70%. Both sides of the curves have steep edges, which define the cut-on and cutoff wavelengths.

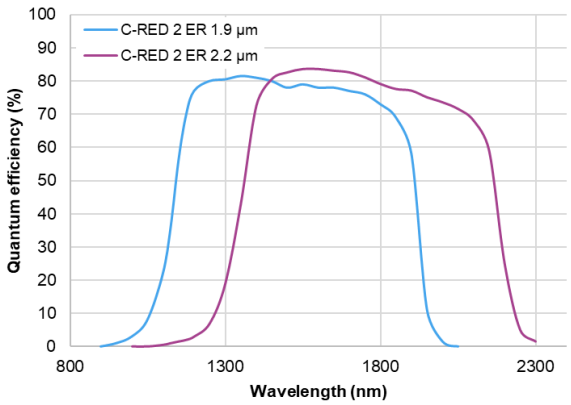

Figure 2. Quantum efficiency at room temperature for the two detectors used in the C-RED 2 ER camera

2.2 Wavelength sensitivity shift with temperature

It is well known that it exists a dependence of the quantum efficiency on the sensor temperature. The energy bandgap of the material depends on the lattice parameter, which is affected by thermal phenomenon. In turn, as the bandgap of the material defines the energy required to generate electrons using the thermo-electric effect, the cutoff wavelengths of detectors drift with temperature. The cut-on is also affected and correspond to the shift of the bandgap of the buffer material that is used to grow the InGaAs sensitive layer.

Figure **3** below illustrates the drift of the low cutoff wavelength that can be observed on a C-RED 2 ER 2.2µm camera. For both the C-RED 2 ER 1.9µm and the C-RED 2 ER 2.2µm, it has been observed that the operating temperature has limited effect on the peak sensitivity value.

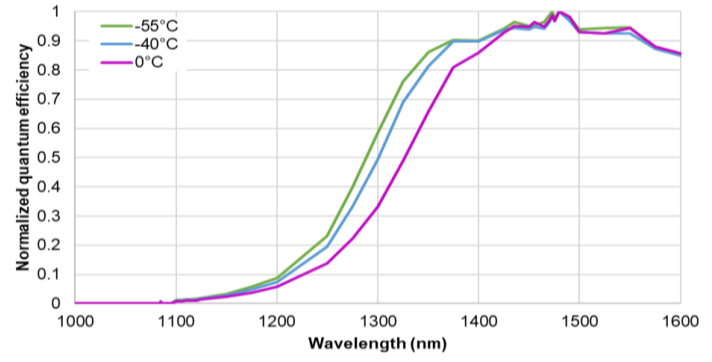

Figure 3. Measured low cut-off wavelength shift as a function of temperature for C-RED 2 ER 2.2 µm (normalized)

4. CAMERA PERFORMANCES

First results have been published in [10], we are now able to provide values with statistical significance and comparison of performances from C-RED 2 ER 1.9µm and C-RED 2 ER 2.2µm. The characterization of the camera performance is always done on raw images.

4.1 Readout noise

Readout noise is evaluated in dark conditions with a cooled sensor, at 50 µs integration time. The contribution of the dark current to the total temporal noise is considered negligeable at low temperature and very short integration times. Typically, the C-RED 2 ER 1.9 µm achieves a median readout noise < 50 e^- while C-RED 2 ER 2.2 µm readout noise is < 40 e^-.

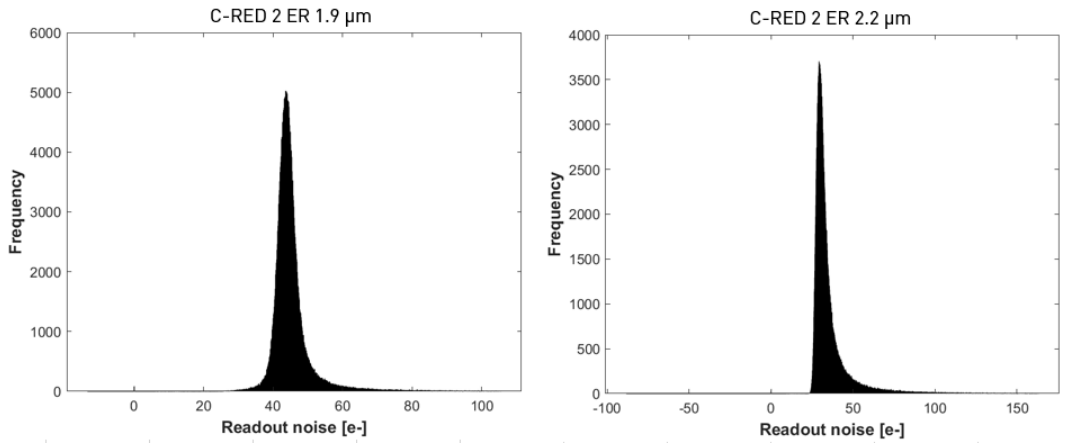

Figure 4. Typical readout noise distributions

4.2 Dark current

Measuring the dark current of cameras sensitive beyond 1.7 µm is not straightforward. The temperature-induced dark signal, in other words the detection of thermal radiations from the surrounding environment, including the camera core, pollutes the measurement of the actual detector dark current. The radiance of a black body at room temperature as a function of wavelength is provided in Figure 5. The fact that extended range cameras are sensitive to the thermal background makes it difficult to isolate the dark current. Here, dark current is evaluated with the contribution of the background thermal emission, from the linear regression of the dark signal of the High gain capacitor as a function of integration time, for a cooled camera looking at a 20°C target. For C-RED 2 ER 2.2 µm, dark signal is typically 120 000 e^-/pixel/s, while for a C-RED 2 ER 1.9 µm it is typically 20 000 e^-/pix/s.

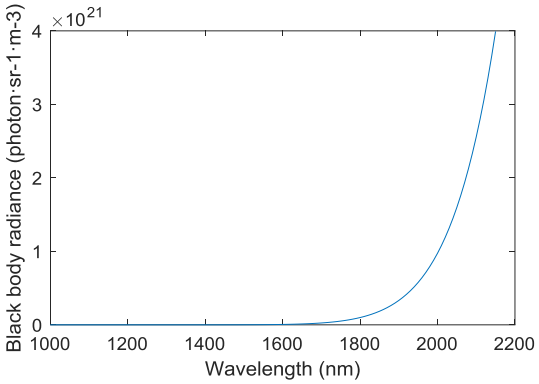

Figure 5 : Spectral density function of thermal black body radiance at 25°C as a function of wavelength.

4.3 Linearity

Linearity is evaluated by exposing the camera to a flat field illumination of fixed intensity and varying the integration time. The response nonlinearity is the deviation from the linear regression in the range of 10 to 90 % of the full well. For both cameras, the typical non-linearity is < 1%. Typical full wells are reported in Table 3.

Table 3. Full well typical values

	High gain	Medium gain	Low gain
C-RED 2 ER 1.9 µm	34 ke^-	132 ke^-	1.53 Me^-
C-RED 2 ER 2.2 µm	34 ke^-	130 ke^-	1.47 Me^-

5. CORRECTING LATTICE-MISMATCH ARTEFACTS

At room temperature (295 K), $In_{0.53}Ga_{0.47}As$ is the alloy composition that offers lattice constant match with InP. The energy bandgap of the resulting semiconductor is 0.75 eV [9]. When the lattice constant mismatch of InGaAs and the InP substrate exceeds a few percent, the strain due to the mismatch induces defects in the structure. Additionally, as mentioned earlier, lattice parameter is a function of temperature. Because the coefficient for the thermal expansion of the material is different for InGaAs and InP, that of InGaAs being significantly larger, lattice-mismatching increases with temperature.

The lattice mismatch artefacts of the extended InGaAs technology can be a major drawback for its use in imaging and sensing applications. The C-RED 2 ER can operate at low temperature, with different readout modes and achieve high-speed frame processing to optimize the output image. The camera is capable of running at 600 full frames per second with image corrections applied.

Figure 6 illustrates the raw cosmetics of the cameras, when operated at water-cooled temperatures and running at full speed. The geometrical patterns resulting from the lattice mismatch can clearly be seen. As expected from the percentage of lattice-mismatching, the C-RED 2 ER 2.2µm is more affected by then the C-RED 2 ER 1.9µm.

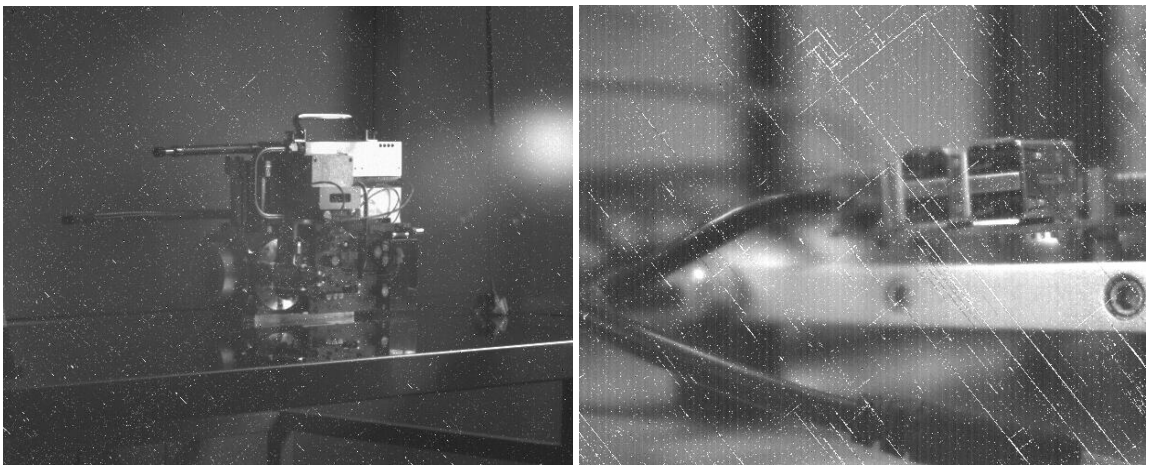

Figure 6. Raw images from the C-RED 2 ER 1.9 µm (left) and C-RED 2 ER 2.2 µm (right)

Applying pixel gain and pixel offset corrections enables to recover useful signal from pixels affected by the artefacts. In the workflow embedded in the camera, pixels either saturated or nailed to null value can be classified as non-operative and corrected using a standard bad pixel correction procedure. The result is illustrated in Figure 7.

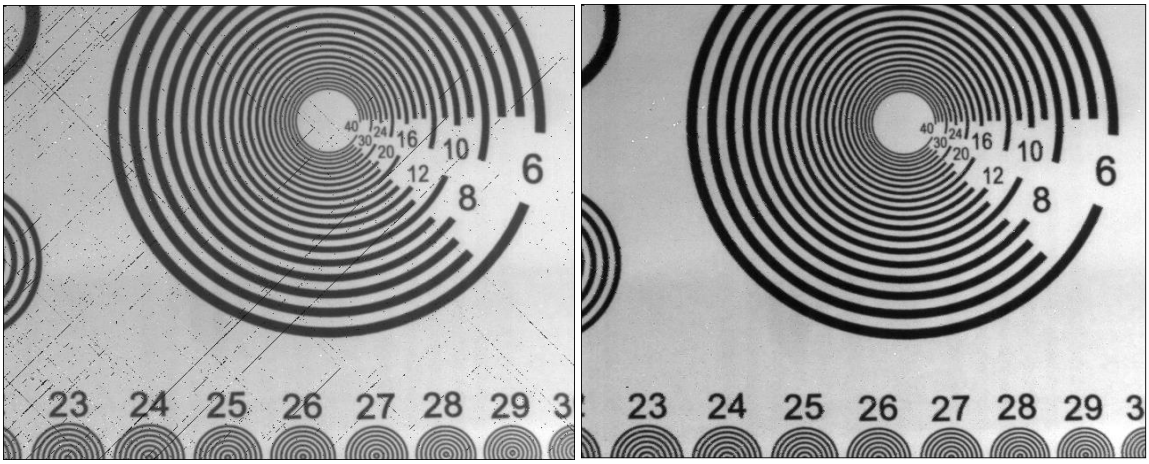

Figure 7 : C-RED 2 ER 2.2µm image after non-uniformity corrections, without (left) and with (right) bad pixel correction

6. CONCLUSION

Sensing and imaging benchtop applications requiring a camera with a sensitivity beyond the standard 1.7 µm cutoff wavelength of InGaAs were limited by the complexity of solutions based on MCT and the lack of performance of alternative solutions. The C-RED 2 ER are extended range InGaAs 640 x 512 high speed cameras that aim to fill in this gap. They can integrate the sensors: BADGER-1.9-T2 and BADGER-2.2-T2, with sensitivity ranges of respectively 1.1 µm to 1.9 µm and 1.2 µm to 2.2 µm. Cooled at -40°C and -55°C, the C-RED 2 ER 1.9µm and C-RED 2 ER 2.2 µm are able to achieve high performance in terms of readout noise, dark current, and readout speed. Additionally, the 2-point non uniformity, lattice-mismatch and bad pixel corrections are embedded in the camera and can be applied without reducing the framerate. We believe that the C-RED 2 ER cameras are good candidates for a use in benchtop laboratory configurations for applications in astronomy, material analysis and biomedical imaging.

REFERENCES

[1] B. Chen, Y. Chen, and Z. Deng, "Recent Advances in High Speed Photodetectors for eSWIR/MWIR/LWIR Applications," *Photonics*, vol. 8, no. 1, p. 14, Jan. 2021, doi: 10.3390/photonics8010014.

[2] D. L. Smith and C. Mailhiot, "Proposal for strained type II superlattice infrared detectors," *J. Appl. Phys.*, vol. 62, no. 2545, 1987, doi: 10.1063/1.339468.

[3] G. A. Sai-Halasz, R. Tsu, and L. Esaki, "A new semiconductor superlattice," *Appl Phys Lett*, vol. 30, no. 651, 1977.

[4] T. Rauch *et al.*, "Near-infrared imaging with quantum-dot-sensitized organic photodiodes," *Nat. Photonics*, vol. 3, no. 6, pp. 332–336, Jun. 2009, doi: 10.1038/nphoton.2009.72.

[5] Thomas P. Pearsall and H. Jr. J.W., "Growth and characterization of lattice- matched epitaxial films of GaxIn1−xAs/InP by liquid- phase epitaxy," *J. Appl. Phys.*, vol. 48, no. 4407, 1977, doi: 10.1063/1.323399.

[6] P. Feautrier *et al.*, "C-RED 2 InGaAs 640x512 600-fps infrared camera for low order wavefront sensing," in *Adaptive Optics Systems VI*, Austin, United States, Jul. 2018, p. 68. doi: 10.1117/12.2313545.

[7] R. K. Gibson, R. Oppenheimer, C. T. Matthews, and G. Vasisht, "Characterization of the C-RED 2: a high-frame rate near-infrared camera," *J. Astron. Telesc. Instrum. Syst.*, vol. 6, no. 01, p. 1, Nov. 2019, doi: 10.1117/1.JATIS.6.1.011002.

[8] A. Rouvié *et al.*, "SWIR InGaAs focal plane arrays in France," 2013, vol. 8704–2.

[9] Y. Takeda, A. Sasaki, Y. Imamura, and T. Takagi, "Electron mobility and energy gap of In0.53Ga0.47As on InP substrate," *J. Appl. Phys.*, vol. 47, no. 5405, 1976, doi: 10.1063/1.322570.

[10] I. De Kernier *et al.*, "C-RED 2 ER: an extended range SWIR camera for hyperspectral imaging," in *Optical Components and Materials XIX*, San Francisco, United States, Mar. 2022, p. 49. doi: 10.1117/12.2624018.